Strain engineering of atomic and electronic structures of few-monolayer-thick GaN

A. V. Kolobov,* P. Fons, Y. Saito, and J. Tominaga
Nanoelectronics Research Institute, National Institute of Advanced Industrial Science and Technology (AIST), 1-1-1 Higashi, Tsukuba 305-8565, Japan

B. Hyot and B. André
Université Grenoble Alpes, CEA, LETI, MINATEC campus, F38054 Grenoble, France

(Received 4 April 2017; published 17 July 2017)

Two-dimensional (2D) semiconductors possess the potential to ultimately minimize the size of devices and concomitantly drastically reduce the corresponding energy consumption. In addition, materials in their atomic-scale limit often possess properties different from their bulk counterparts paving the way to conceptually novel devices. While graphene and 2D transition-metal dichalcogenides remain the most studied materials, significant interest also exists in the fabrication of atomically thin structures from traditionally 3D semiconductors such as GaN. While in the monolayer limit GaN possesses a graphenelike structure and an indirect band gap, it was recently demonstrated that few-layer GaN acquires a Haeckelite structure in the direction of growth with an effectively direct gap. In this work, we demonstrate the possibility of strain engineering of the atomic and electronic structure of few-monolayer-thick GaN structures, which opens new avenues for their practical application in flexible nanoelectronics and nano-optoelectronics. Our simulations further suggest that due to the weak van der Waals-like interaction between a substrate and an overlayer, the use of a MoS_2 substrate may be a promising route to fabricate few-monolayer Haeckelite GaN experimentally.

DOI: 10.1103/PhysRevMaterials.1.024003

I. INTRODUCTION

Most materials that we encounter today exist in their three-dimensional—or bulk—form, i.e., their dimensions exceed their lattice constant in all three dimensions. An exception is man-made heterostructures, where the thicknesses of individual materials, e.g., Si and Ge in case of Si/Ge or, say, GaAs and AlAs in case of GaAs/AlAs nanostructures, can be as small as a few nanometers resulting in the formation of a 2D electron gas in structures such as quantum wells. Such structures are usually fabricated using (hetero)epitaxy, where the growth mode of an overlayer is determined by the structure of the preceding layer (substrate). As a consequence, the overlayer and the substrate are covalently bonded and there is inevitably interdiffusion that broadens the interfaces. The formation of truly two-dimensional structures with atomically flat interfaces remained a challenge that has been solved with the advent of graphene.

Graphene is a single layer of graphite, i.e., it possesses a two-dimensional honeycomb arrangement of carbon atoms. At the same time, the characteristics of graphene are very different from those of graphite, which is the corresponding three-dimensional arrangement of carbon. In particular, it can support an electrical current density six orders of magnitude larger than copper, it is the best known conductor of heat, it is the lightest material known and also the strongest material known. Being atomically thin, graphene is naturally transparent. These properties of graphene make it a very promising material for a variety of applications ranging from ultrafast electronics to bionic devices.

Following the success of graphene, other two-dimensional (2D) materials, such as transition-metal dichalcogenides (TMDC) with the generic formula of MX_2 (M = Mo, W; X = S, Se, Te) have emerged as very promising materials. Usually, 2D materials possess a layered structure, where atomically thin covalently bonded layers (often referred to as monolayers) are held together by weak van der Waals (vdW) forces. Consequently, mono- and few-layer structures made of such materials can be easily prepared. It should be also noted that, similar to graphene, the properties of monolayer-thick TMDC films are also different from their bulk counterparts. Thus, while bulk TMDCs are indirect gap materials, monolayer TMDCs possess a direct gap [1,2] and extraordinary large exciton and trion binding energies [3–5], which makes them efficient competitors for conventional III-V optoelectronics. The ultimately small thickness of TMDC make them (i) extremely energy efficient and (ii) suitable for transparent and flexible optoelectronics [6].

The progress achieved with 2D semiconductors has triggered increased interest in atomically thin layers of conventional, i.e., nominally three-dimensional, III-V semiconductors. Bulk III-V compound semiconductors, such as GaAs, AlAs, InAs, InP, GaN, and their ternary and quaternary alloys are direct-gap materials with the resulting ability to efficiently emit and detect light, which makes them ideal for uses in lasers, light-emitting diodes and optical detectors. In most current applications, III-V semiconductors with the characteristic dimensions of several nanometers, i.e., approximately ten or more lattice constants are used.

III-V semiconductors are fundamentally different from the easily cleaved vdW solids. Because these materials in their bulk form are tetrahedrally bonded with all atoms being sp^3 hybridized, the surfaces contain a large number of dangling bonds making them unstable. In addition, in binary crystals, due to the different electronegativity of the constituent species, the two opposing surfaces associated with "cleavage" into hexagonal layers (0001 and $000\bar{1}$) are polar,

*a.kolobov@aist.go.jp

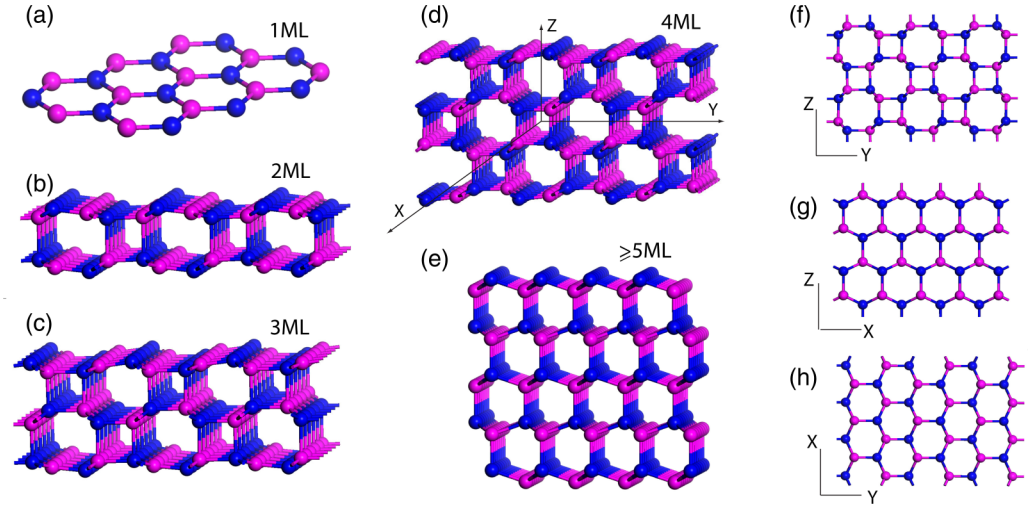

FIG. 1. The lowest energy structures of thin GaN slabs. While a monolayer-thick GaN (N: blue, Ga: magenta) acquires the graphitic phase (a), a Haeckelite phase is established for 2ML (b), 3ML (c), and 4 ML (d), while 5ML and thicker slabs remain in the wurtzite phase (e). (f)–(h) show three different projections for the Haeckelite phase. Note that the axes have the same notations as in (d), where a 3D view of a 4ML-thick layer is shown.

i.e., formed by cations and anions (type-III surfaces according to Tasker's classification [7]) and are intrinsically unstable due to the divergence of the surface energy. Such surfaces can be stabilized through different processes, such as vacancy formation, surface reconstruction, and charge transfer from the cation surface to the anion surface [8–10]. An alternative mechanism for stabilization of monolayer wurtzite structures, e.g., GaN, is the formation of planar graphenelike structures. In this case, the cations and anions are arranged in a trigonal-planar configuration, which serves to remove the surface dipole moment and consequently to stabilize the film [11].

It was proposed that planar graphitelike structures are energetically more favourable also for few-layer GaN structures [11–13]. Subsequent studies using both structure relaxation and phonon simulations, however, demonstrated that graphitic few-layer GaN structures are intrinsically unstable (being a saddle point in configuration space) and reconstruct into a Haeckelite phase [14] with a 4|8 bonding pattern and alternating shorter and longer Ga-N interatomic distances along the growth direction [15].

Figures 1(a)–1(e) show structures of mono- and few-layer GaN slabs. As already mentioned, the 1ML structure is graphenelike [Fig. 1(a)], while 2ML–4ML structures [Figs. 1(b)–1(d)] possess a Haeckelite phase [15]. 5MLs [Fig. 1(e)] and thicker slabs retain the wurtzite structure of the bulk although the interplane distances slightly increase towards the surfaces. To give the readers a better idea of the Haeckelite phase, Figs. 1(f)–1(h) show the ideal Haeckelite structure of the hypothetical bulk phase in three different projections with the axes having the same notations as shown in Fig. 1(d) for a 4ML slab. Along the X axis the structure has square and octagonal channels while along the Y and Z axes it is hexagonal. It can be seen that, different from the polar wurtzite phase, dipoles in the Haeckelite phase cancel out, which is the underlying reason for this phase to be energetically favourable for thin slabs, where the surface dipoles are a destabilizing force for the wurtzite phase. It may also be noted that while in the bulk Haeckelite phase all Ga-N bonds are oriented along the Y and Z axes [Fig. 1(f)], in the few-layer limit the planarity of the surfaces is perturbed [as can be seen in Fig. 2 (top)] for an example of a 2ML slab.

As was noted in the previous work [15], while the 1ML graphitic phase of GaN is characterized by an indirect gap, which significantly reduces its application potential from an optoelectronic perspective, the Haeckelite structures possess an effectively direct band gap, which makes them promising candidates for applications in (flexible) optoelectronic devices. It may be interesting to note that the trend is different between vdW bonded TMDC and covalently bonded III-V semiconductors: in the former the indirect gap in the bulk phase transforms into a direct gap in the monolayer limit [1,2].

Recent progress in GaN epitaxial growth on graphene [16–24], a perfectly flat material that does not possess any dangling bonds (and thus minimizing the chemical interaction between the substrate and the overlayer) opens interesting

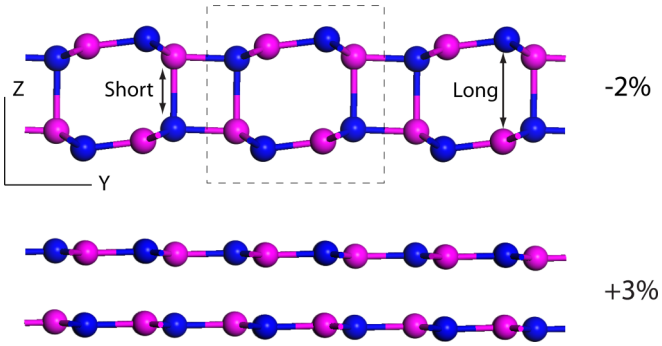

FIG. 2. Changes in the atomic structure of 2ML GaN induced by strain. While the compressed (or relaxed) structure is buckled Haeckelite (upper) with two distinctly different Ga-N interlayer distances, it changes to planar graphitic under tensile strain (lower). The dashed line shows the unit cell.

opportunities in this direction. In most previous reports, however, the thickness of GaN exceeded the critical thickness of 5 ML and consequently the structure of the grown GaN was wurtzite [17,19–22]. An interesting exception was reported in Ref. [25]. In this work, the authors obtained few-layer GaN by heating few-layer flakes of GaS and/or GaSe in ammonia at approximately 650 °C. Because the starting materials possess micalike morphology, nanosheets could be potentially fabricated by micromechanical cleavage. Of special interest is a recent work on the graphene stabilization of few-ML-thick GaN using a migration enhanced encapsulated growth technique [26]. The structure of the grown GaN was found not to be flat and additionally bond polarity inversion in the 2D GaN [26] with respect to the bulk wurtzite phase was observed, which—we believe—may well be an indication of the formation of the 8|4 Haeckelite phase.

Elastic strain has long been known to be a powerful tool to tune materials properties alongside with alloying. However, elastic strain engineering of traditional bulk semiconductors has been in practice very limited due to the fact that traditional materials usually cannot sustain elastic shear strain or tensile strain exceeding 0.2%–0.3% before inelastic relaxations set in. The situation drastically changed with the advent of nanotechnology. Nanomaterials are mechanically much stronger than their bulk counterparts and as a consequence one can apply far greater shear or tensile stresses to tune their electronic, magnetic, optical or plasmonic, ionic, phononic, thermoelectric, or catalytic properties, such as band gap, carrier mobility, superconducting transition temperature, etc. [27]. This ability of nanomaterials to withstand much greater strain has been formulated as "smaller is stronger" [28] and has opened a window of opportunities to a vast space for development of new materials and devices.

One of the best known examples of successful practical application of strain engineering is strained silicon technology, where biaxial or uniaxial tensile strain up to a few percents is applied to a 10–100-nm wide silicon channel (e.g., by epitaxial strain to a $Si_{1-x}Ge_x$ substrate) resulting in a dramatic increase in carrier mobility. Thus in addition to just silicon, it is now possible to fabricate 1% strained, 2% strained, etc., silicon, each material possessing distinctly different properties.

Atomically thin, two-dimensional (2D) semiconductors are champions as to the strain that can be applied to them. Thus using AFM, indentation on free-standing graphene suspended on top of a micrometer-sized hole was performed [29] and from these measurements a biaxial tensile elastic strain limit of 25% was extracted. An atomic monolayer of MoS_2, a model 2D transition metal dichalcogenide, could be stretched elastically to 11% experimentally [30] resulting in drastic changes of the electronic structure. Application of strain has also been demonstrated to induce a $2H$-$1T'$ phase transition in TMDC [31]. Strain engineering was also proposed as an effective tool to control a transition between topologically nontrivial to topologically nontrivial phases in layered chalcogenides [32–35] as well as phase transformation in so-called interfacial phase change materials that are made from short-period 2D superlattices of GeTe and Sb_2Te_3 [36]. It is thus extremely interesting to investigate the effect of applied strain on atomic and electronic structure of few-ML-thick layers of GaN and this is what we performed in this work.

II. SIMULATION DETAILS

Density-functional calculations were carried out at 0 K using the plane-wave codes CASTEP [37]. A 15-Å vacuum layer was used to separate periodic replicas. Ultrasoft pseudopotentials were used for Ga and N atoms. The Ga and N pseudopotential included the Ga $3d^{10}4s^24p^1$ and N $2s^22p^3$ as valence electrons, respectively. The exchange term was evaluated using the generalized gradient approximation (GGA) and the PBE functional [38] as implemented in CASTEP. A plane-wave cutoff energy of 295 eV and a $4 \times 4 \times 1$ Monkhorst-Pack grid were used. The simultaneous convergence criteria were set to the following values: energy: 5×10^{-6} eV/atom, max. force: 0.01 eV Å^{-1}, max. stress: 0.02 GPa, max. displacement: 5×10^{-4} Å. The Broyden-Fletcher-Goldfarb-Shanno (BFGS) optimization algorithm was used. Grimme's DFT-D2 method [39] was used to account for vdW interactions. The structural relaxation was performed under conditions, where

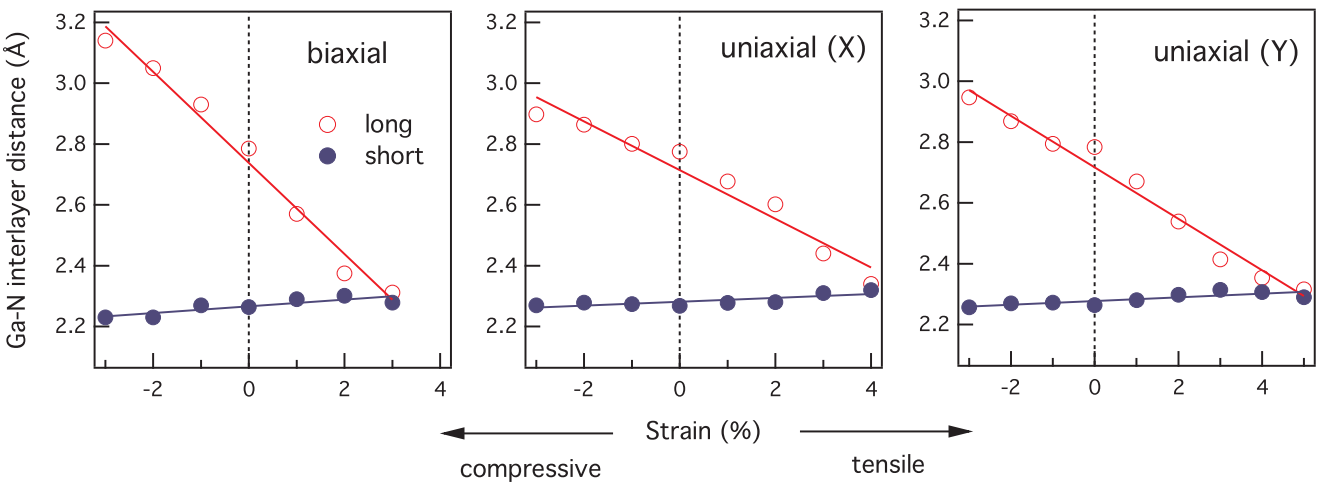

FIG. 3. Variations of the shorter and longer Ga-N interatomic/interplane distances for a 2ML GaN slab under biaxial (left) and uniaxial strain applied along the X (middle) and Y (right) axes. Note that positive strain values correspond to tensile strain.

both the atomic position within the cell and the cell size were allowed to vary. The atom-projected band structures were computed using VASP in conjunction with the python-based PYMATGEN library [40].

Band structures were additionally calculated using WIEN2K [41]. WIEN2K is an all electron code that uses a linearized augmented plane wave + local orbital (LAPW+lo) basis within density-functional theory; the PBE functional was used. A Monkhorst-Pack grid of $7 \times 7 \times 1$ was used for integrations in the Brillouin zone and a $R_{\mathrm{mt}}K_{\mathrm{max}} = 7.0$ value was used for the plane-wave component of the plane-wave basis used between augmentation spheres. To achieve better agreement of the simulated energy gap with experimental values we have additionally used WIEN2K with the modified Beck-Johnson potential [42] within the LDA approximation [43].

III. RESULTS AND DISCUSSION

Figure 2 demonstrates the effect of strain on the structure for the example of 2ML-thick GaN. It can be seen that while application of compressive strain preserves the Haeckelite structure with two distinctly different (short and long) interlayer Ga-N distances (upper panel), this difference gradually decreases and disappears upon application of tensile strain (lower panel) with the material acquiring a "flat" geometry. The behavior is qualitatively similar in 2ML–4ML-thick slabs, while the extent of the structural change is larger in thinner slabs as will be demonstrated below.

The Ga-N distance change as a function of applied strain, both biaxial and uniaxial, is shown in Fig. 3. One can see that in all cases the strain has a rather small effect on the shorter Ga-N distances corresponding to the Ga-N covalent bonds, while the longer distances across the octagonal channels change more significantly. From a comparison of the panels, one can also see (i) that the effect of bipolar strain is stronger than that of unipolar strain and also that (ii) the direction of the unipolar strain has a very weak effect.

The strain-induced changes in the band structure for a 2ML-thick slab simulated using CASTEP with GGA-PBE are shown in Fig. 4 (bottom). The notations for the k points and the reciprocal lattice are shown in the upper panel of the same figure.

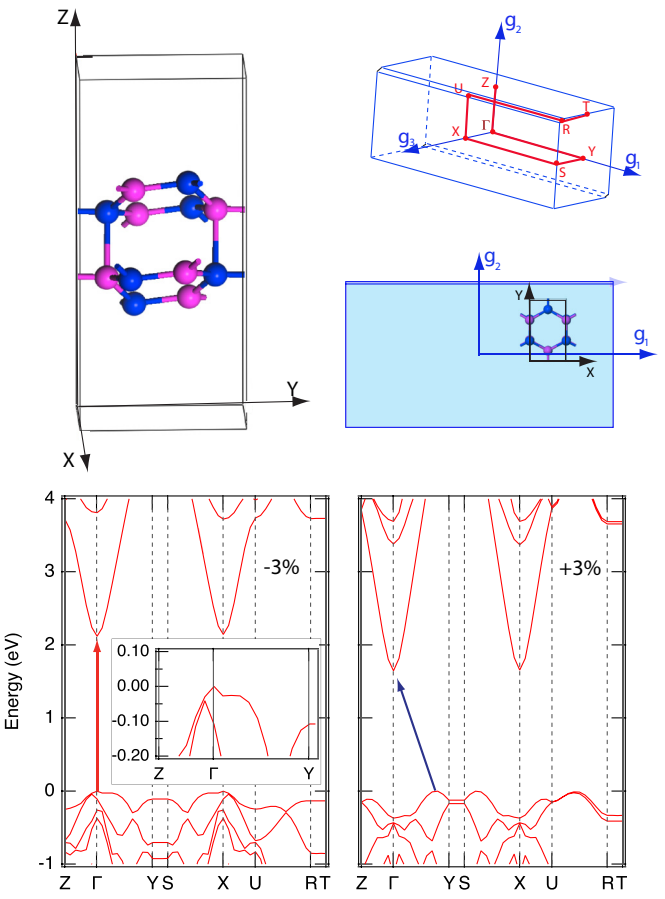

FIG. 4. (Top) The unit cell (left), reciprocal lattice (upper right), and the relationship between the two (lower right) for a 2ML slab. (Bottom) Band structures of 2ML-thick GaN under a compressive (left) and tensile (right) strain of 3% simulated using GGA-PBE. The inset in the left panel shows the details of the band structure of the valence band near the Γ point. Note that the band gap is direct in the compressed state.

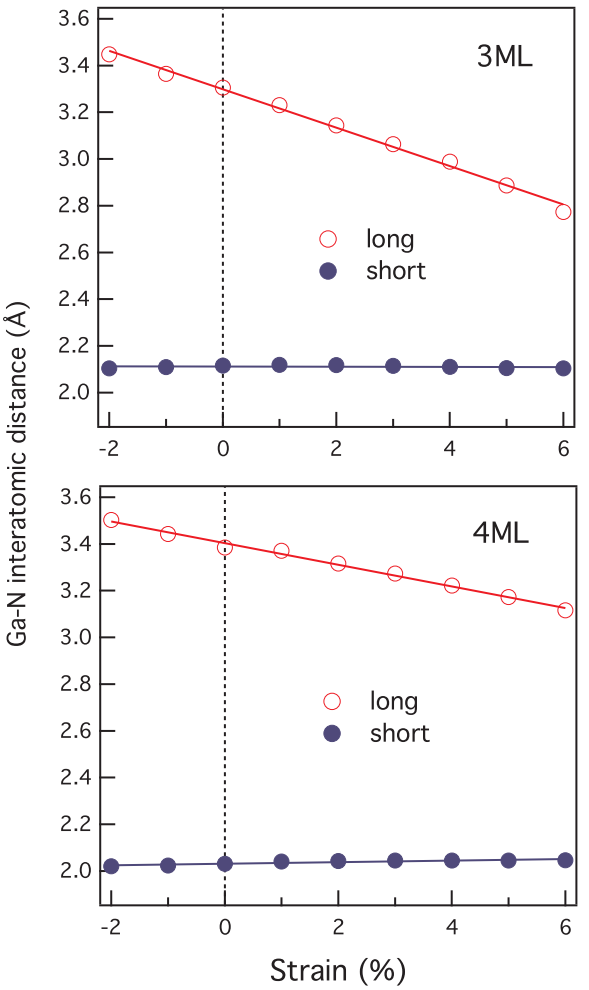

FIG. 5. Variations of the shorter and longer Ga-N interatomic/interplane distances for 3ML (upper) and 4ML (lower) GaN slab under biaxial strain.

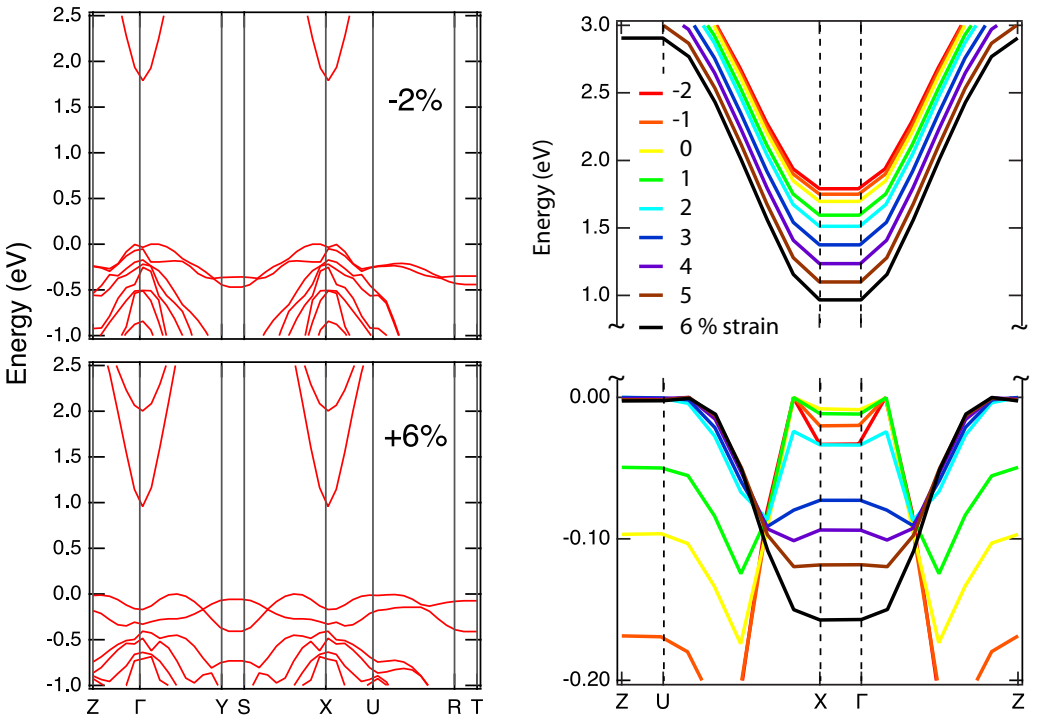

FIG. 6. (Left) Band structures of 4ML GaN under 2% compressive strain (top) and 6% tensile strain (bottom). Right panel: Evolution of the lowest conduction band and the uppermost valence band of 4ML GaN neat the Γ point under applied strain. Note that the scales for the conduction and valence bands in the right panel are significantly different.

The following observations can be made. The most important change is a transition from an indirect gap under tensile strain to a direct gap with compressive strain. It should also be noted that there is a pronounced decrease in the band gap, mainly associated with the lowering of the conduction-band minimum. It is also interesting to note that while the lowest conduction band monotonically shifts down in energy upon increased tensile strain, the uppermost valence band exhibits significant dispersion changes.

More accurate calculations of the band structure using the all-electron code WIEN2K have shown that the structure does not acquire a direct gap strictly speaking (see Ref. [44], Fig. 1S). However, these result unambiguously demonstrate that the valence-band maximum at the Γ point moves up in energy upon application of compressive strain; the difference between the direct and indirect gaps in the WIEN2K simulation was on the order of 0.05 eV, i.e., for devices operating at room temperature or above the band gap is effectively direct. Similar studies of thicker slabs have shown that in 3ML- and 4 ML-thick layers, the layer "flattening" proceeds much more slowly and the noticeable difference between the shorter and longer Ga-N distances is preserved at tensile strains exceeding 6% (Fig. 5).

Figure 6 (left panels) shows the band structure of the 4ML slab simulated using CASTEP. As in the case of the 2ML slab, the decrease in the band gap is due to a monotonic downwards shift of the conduction band. Also, similar to the case of the 2ML slab, the dispersion of the conduction band remains essentially unchanged while that of the valence band changes drastically. Especially interesting is the behavior around the Z and Γ points, which is shown in Fig. 6 (right panel), where we have chosen a different path to better illustrate the previous statement. This panel shows the lowest conduction band and the uppermost valence band. Note that the energy scales for the valence and conduction bands in Fig. 6 (right panel) are very different. One can clearly see a nonmonotonic behavior of the valence-band maximum with strain at the Γ (and X) and Z (and U) points, as is additionally illustrated in Fig. 7. In particular, a clear change in the trend is observed at strains ca. $+1\%$. It is also interesting to note that while the valence-band maximum at the Z-point levels off for strains $\geqslant 2\%$, the variation at the Γ

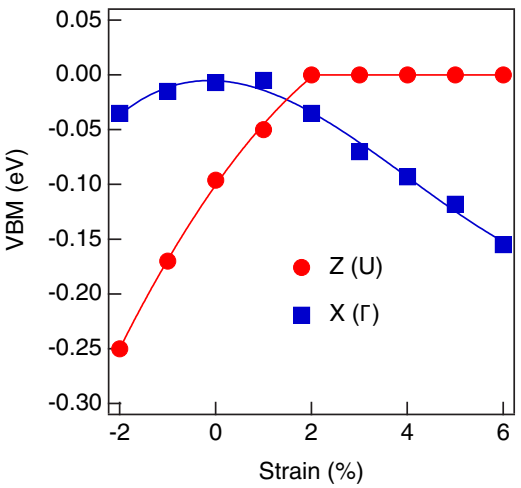

FIG. 7. Variation of the valence-band maxima at the $Z(U)$ and $X(\Gamma)$ points with strain.

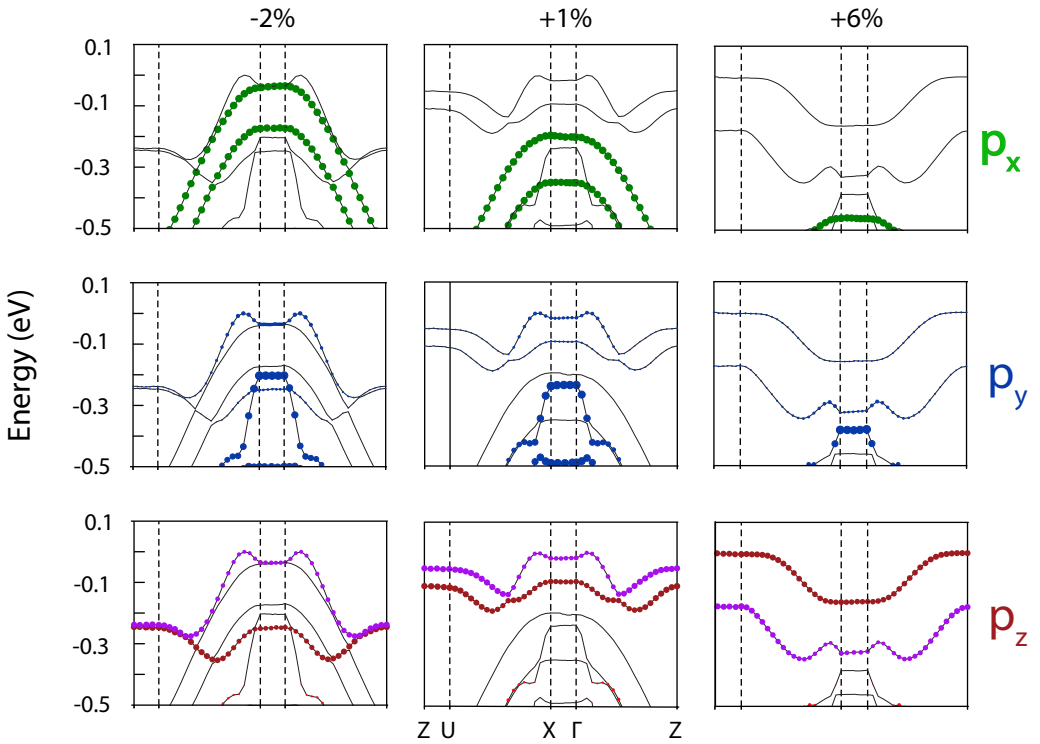

FIG. 8. Atomic orbital projected valence-band structures of 4ML GaN as a function of strain from -2% to $+6\%$ as marked at the top of the figure. Contributions from the N p_x (green), p_y (blue), and p_z (red/purple) orbitals are shown in the upper, middle, and lower panels, respectively. The two upper bands that are predominantly due the p_z orbitals (lower panel) are shown in two different colours (red and purple) to make clear the complicated band evolution under strain. The size of the coloured dots corresponds to the relative weight of particular states for the shown bands at various k points.

point has the largest gradient in this strain range. In contrast, while the variation at the Γ point is the largest in the -2% to $+2\%$ range, the change at the Z point is almost negligible.

To gain more insight, we simulated the atomic orbital projected band structures. The results, shown in Fig. 8, demonstrate that while for negative strain the top of the valence band is dominated by N p_x states, with p_y and p_z states having smaller contributions, the top of the valence band is exclusively due to the N p_z states for larger positive strains. It is further visible that while the bands associated with the N p_x and p_y states monotonically decrease in energy when the strain varies from -2% to $+6\%$, those associated with the N p_z states exhibit over the same strain range a more complicated behavior, demonstrating that the most significant changes in the band structure are due to interatomic interactions along the z axis, which change as the structure is transformed from the Haeckelite 3D to a layered 2D phase. In particular, while the two highest bands associated with the p_z states are degenerate at Z for negative strain (Fig. 8, lower panel), the degeneracy is lifted when the strain changes from negative to positive. Furthermore, the order of these bands inverts under the same conditions (the $\mathcal{M}$-shaped band is higher in energy for -2% and lower in energy for $+6\%$ strain). Based on these results, we can conclude that the transition from the indirect gap at positive strains towards the direct gap at negative strains is due to an increase in energy of the N p_x states.

We note that in the band structures shown in Fig. 8, the two upper valence bands are degenerate at Γ for -2% strain with the two small bumps located to the right of the Γ and to the left of the X point (as shown in Fig. 8) preventing the structure from acquiring a true direct gap. At the same time, the band associated with N p_x states moves down in energy lifting this degeneracy as the compressive strain is reduced and subsequently changes to tensile. In order to check whether the observed degeneracy at -2% compressive strain, limiting the indirect-to-direct gap transformation, is an intrinsic property of the Haeckelite phase or a mere coincidence, we performed additional simulations for a larger compressive strain of -5%. The result, shown in Fig. 9, where the color scheme of Fig. 8 has been preserved, unambiguously demonstrates that increasing the compressive strain further pushes the N p_x upwards in energy resulting in the formation of a genuine direct band gap at the Γ point. In the lower panel, we additionally show the atomic structure of the 4ML GaN slab at -5% strain. One can see that while the Haeckelite phase is preserved, there are rather strong distortions, especially towards the slab surfaces, with the N atoms being somewhat pushed out forming the outermost atomic plane, similar to the case of the 2ML slab (cf. Fig. 2).

As a way to obtain a band gap value comparable with the experimental values, we have additionally calculated the band structure using WIEN2K with the somewhat more "expensive" modified Becke-Johnson (mBJ) potential [42], the use of which is known to produce band gaps rather close to experiment [43,45]. The result is shown in Fig. 10 (left panel). From comparison of the band structures obtained using the GGA-PBE and mBJ functionals (Fig. 4 versus Fig. 10) one

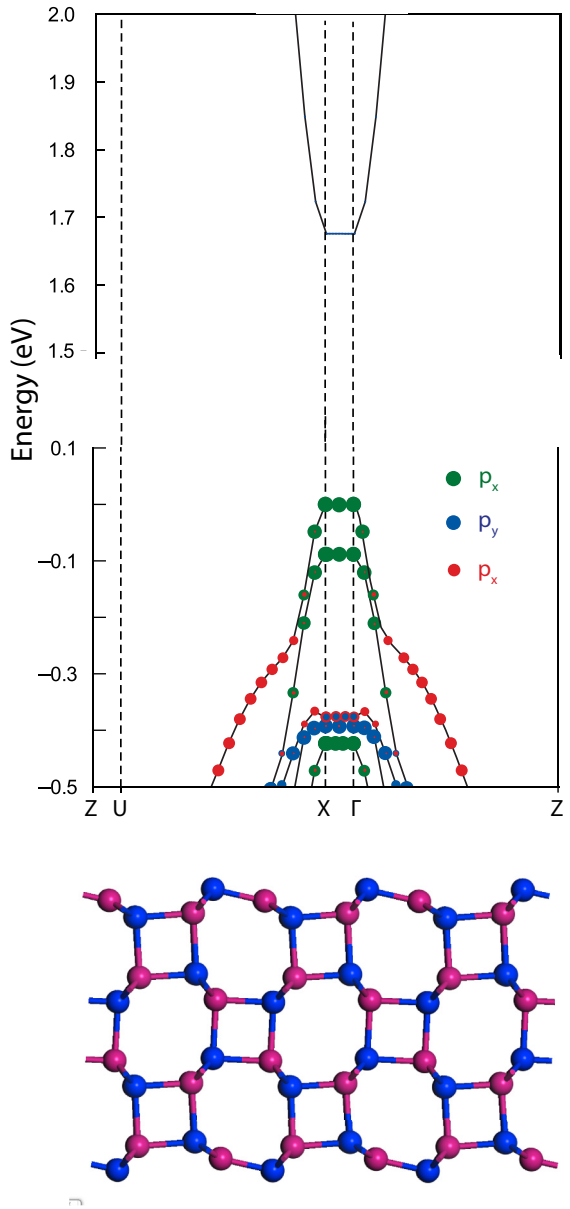

FIG. 9. (Top) Atomic orbital projected band structure of 4ML GaN for −5% compressive strain. Contributions from the N p_x, p_y, and p_z orbitals are shown in green, blue, and red, respectively. One can clearly see the formation of a direct gap due to the p_x orbitals. Note that the energy scales for the valence and conduction bands are very different. (Bottom) Atomic structure of 4ML GaN at −5% strain.

can see that the main difference between the two is a larger gap (approximately 3.2 eV) for the case of the mBJ potential with other details of the band structure being nearly identical. For reference, the band gap of bulk GaN calculated using the mBJ potential (Fig. 10, right panel) yielded a value of 3.3 eV, which compares well with the experimental value of 3.4 eV. The inclusion of spin-orbit coupling did not have any effect, which is not surprising considering that both Ga and especially N are light elements.

Figure 11 shows the strain dependence of the band gap simulated using the mBJ functional. In all cases, the band

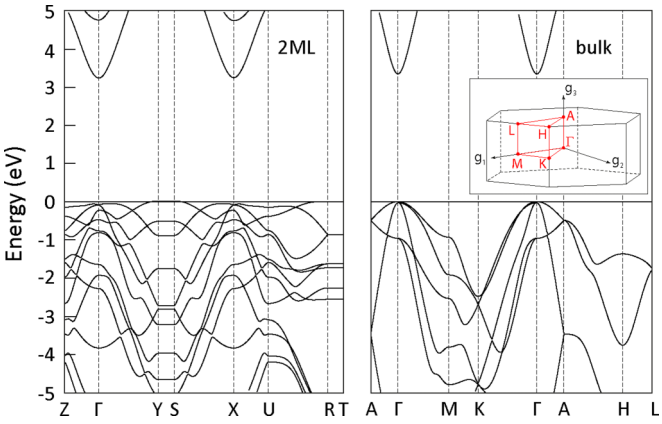

FIG. 10. Band structures of a 2ML slab (left) and bulk (right) GaN calculated using WIEN2K and mBJ potential. The inset to the right panel shows the reciprocal unit cell of bulk (wurtzite) GaN.

gap decreases for tensile strain. Very similar results were obtained using GGA-PBE (see Ref. [44], Fig. 2S) except for the absolute values of the band gaps. In addition, one can see that the band gap decreases for thicker slabs. Since the existing 2D (transition-metal dichalcogenide) semiconductors typically possess forbidden gaps of typically less than 2 eV, the addition of (approximately 3 eV) wide-gap few-ML GaN to the class of 2D semiconductors will significantly broaden the application potential of 2D nano-optoelectronics.

Finally, we would like to note here that while the reported results refer to free-standing GaN slabs, use of atomically flat and inert substrates is a promising route to fabricate the few-ML GaN structures experimentally. Growth of few ML on graphene has recently been reported [16–24,46].

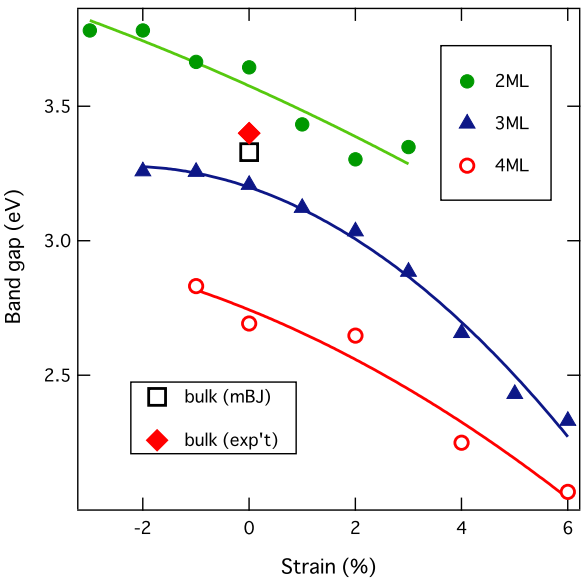

FIG. 11. Strain dependence of the band gap in few-monolayer GaN calculated using mBJ functional. For comparison, the value for bulk GaN calculated using the same procedure is also shown alongside with the experimental value of the bulk band gap. The solid lines are guides for the eye.

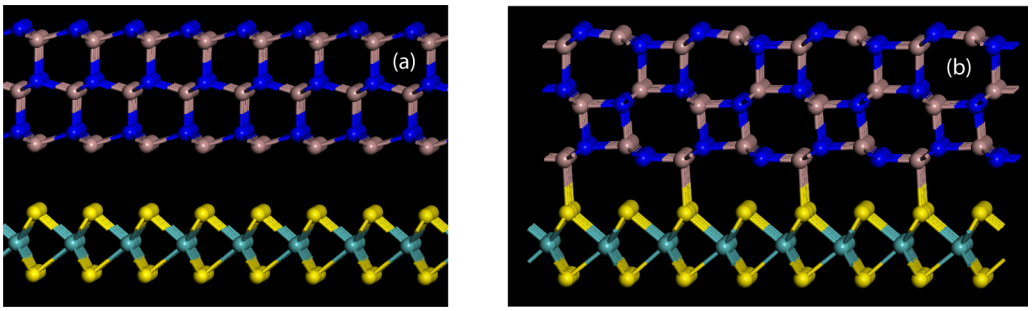

FIG. 12. Starting (a) and relaxed (b) 3ML-thick GaN on MoS_2. Mo atoms are shown in light blue and S atoms are yellow. The result demonstrates that the presence of a (properly chosen) substrate does not affect the formation of the Haeckelite phase of GaN in the few-ML limit.

We propose that epitaxial growth of GaN on transition-metal dichalcogenides may be an alternative route to fabricate such structures. MoS_2 may be especially promising because the lattice parameters of GaN and MoS_2 match very well (while for GaN and graphene there is an ∼30% lattice mismatch [47]) and also MoS_2 possesses an atomically flat saturated surface similar to graphene [48–50], which allows one to expect very weak van der Waals like interaction in the GaN-MoS_2 heterostructure. The semiconducting nature of MoS_2 may present advantages for certain devices compared to graphene. To verify this idea, we performed *ab initio* simulations on a 3ML GaN-MoS_2 heterostructure. Figure 12(b) shows a relaxed GaN-MoS_2 heterostructure [the starting structure for GaN in this calculation was a slice of the wurtzite phase as shown in Fig. 12(a)] obtained using CASTEP and GGA-PBE. This result unambiguously demonstrates that the Haeckelite phase can be acquired by a few-ML GaN even in presence of a (properly selected) substrate. We believe that the presence of weak van-der-Waals-like interaction, which does not lead to a strong effect of the substrate structure on the overgrown layer, is crucial in order to prevent the formation of the wurtzite phase at the initial stages of growth. A systematic *ab initio* study of GaN-MoS_2 heterostructures and superlattices is currently underway and the results will be reported elsewhere.

IV. CONCLUSIONS

In this work, we performed a comprehensive *ab initio* study of the effect of in-plane strain on the atomic and electronic structure of few-ML GaN. Our results demonstrate that while at ambient conditions and under compressive strains the structure is Haeckelite, it gradually transforms to planar upon application of tensile strain. Biaxial strain was shown to have a stronger effect than uniaxial strain, in the latter case the direction of the applied strain has little effect. The changes in the atomic structure are accompanied by drastic changes in the electronic structure, such as the transformation towards a direct gap at compressive strain accompanied by an increase in the band gap due to the upshifting of the conduction-band minimum. At the same time, the structure of the valence band undergoes significant changes with some of the k points effectively flipping in energy. Our simulations demonstrate that the transformation towards a direct gap at negative strains is caused by the increase in energy at the Γ point of the valence band associated with the N p_x states.

The observed results demonstrate that strain is an effective tool to modify the atomic and electronic structure of few-ML-thick GaN, the use of which will lead to the development of novel devices based on this technologically important material. Our results suggest that due to the presence of weak van der Waals interactions the use of a MoS_2 substrate may be an effective tool to realize the few-ML-thick Haeckelite GaN experimentally. The ultimately small thicknesses of the active layer in such devices as opposed to their 3D counterparts will serve to significantly decrease energy consumption. Moreover, the addition of wide-band-gap 2D few-ML GaN to the existing class of 2D semiconductors will significantly extend the potential of 2D nano-optoelectronics.

ACKNOWLEDGMENT

A part of this work was supported by JSPS KAKENHI Grant No. JP16K04896.

[1] K. F. Mak, C. Lee, J. Hone, J. Shan, and T. F. Heinz, Phys. Rev. Lett. **105**, 136805 (2010).
[2] A. Splendiani, L. Sun, Y. Zhang, T. Li, J. Kim, C.-Y. Chim, G. Galli, and F. Wang, Nano Lett. **10**, 1271 (2010).
[3] A. Ramasubramaniam, Phys. Rev. B **86**, 115409 (2012).
[4] A. Chernikov, T. C. Berkelbach, H. M. Hill, A. Rigosi, Y. Li, O. B. Aslan, D. R. Reichman, M. S. Hybertsen, and T. F. Heinz, Phys. Rev. Lett. **113**, 076802 (2014).
[5] K. F. Mak, K. He, C. Lee, G. H. Lee, J. Hone, T. F. Heinz, and J. Shan, Nat. Mater. **12**, 207 (2013).
[6] Q. H. Wang, K. Kalantar-Zadeh, A. Kis, J. N. Coleman, and M. S. Strano, Nat. Nanotechnol. **7**, 699 (2012).
[7] P. W. Tasker, J. Phys. C: Solid State Phys. **12**, 4977 (1979).
[8] J. Fritsch, O. F. Sankey, K. E. Schmidt, and J. B. Page, Phys. Rev. B **57**, 15360 (1998).
[9] J. E. Northrup, R. Di Felice, and J. Neugebauer, Phys. Rev. B **55**, 13878 (1997).
[10] A. Wander, F. Schedin, P. Steadman, A. Norris, R. McGrath, T. S. Turner, G. Thornton, and N. M. Harrison, Phys. Rev. Lett. **86**, 3811 (2001).

[11] C. L. Freeman, F. Claeyssens, N. L. Allan, and J. H. Harding, Phys. Rev. Lett. **96**, 066102 (2006).

[12] H. Şahin, S. Cahangirov, M. Topsakal, E. Bekaroglu, E. Akturk, R. T. Senger, and S. Ciraci, Phys. Rev. B **80**, 155453 (2009).

[13] D. Xu, H. He, R. Pandey, and S. P. Karna, J. Phys.: Condens. Matter **25**, 345302 (2013).

[14] D. C. Camacho-Mojica and F. López-Urías, Sci. Rep. **5**, 17902 (2015).

[15] A. V. Kolobov, P. Fons, J. Tominaga, B. Hyot, and B. André, Nano Lett. **16**, 4849 (2016).

[16] K. Chung, C.-H. Lee, and G.-C. Yi, Science **330**, 655 (2010).

[17] J. Kim, C. Bayram, H. Park, C.-W. Cheng, C. Dimitrakopoulos, J. A. Ott, K. B. Reuter, S. W. Bedell, and D. K. Sadana, Nat. Commun. **5**, 4836 (2014).

[18] T. H. Seo, A. H. Park, S. Park, Y. H. Kim, G. H. Lee, M. J. Kim, M. S. Jeong, Y. H. Lee, Y.-B. Hahn, and E.-K. Suh, Sci. Rep. **5**, 7747 (2015).

[19] L. Zhang, X. Li, Y. Shao, J. Yu, Y. Wu, X. Hao, Z. Yin, Y. Dai, Y. Tian, Q. Huo *et al.*, ACS Appl. Mater. Interfaces **7**, 4504 (2015).

[20] K. Chung, H. Beak, Y. Tchoe, H. Oh, H. Yoo, M. Kim, and G.-C. Yi, APL Mater. **2**, 092512 (2014).

[21] T. Araki, S. Uchimura, J. Sakaguchi, Y. Nanishi, T. Fujishima, A. Hsu, K. K. Kim, T. Palacios, A. Pesquera, A. Centeno *et al.*, Appl. Phys. Express **7**, 071001 (2014).

[22] N. Nepal, V. D. Wheeler, T. J. Anderson, F. J. Kub, M. A. Mastro, R. L. Myers-Ward, S. B. Qadri, J. A. Freitas, S. C. Hernandez, L. O. Nyakiti *et al.*, Appl. Phys. Express **6**, 061003 (2013).

[23] S. J. Chae, Y. H. Kim, T. H. Seo, D. L. Duong, S. M. Lee, M. H. Park, E. S. Kim, J. J. Bae, S. Y. Lee, H. Jeong *et al.*, RSC Adv. **5**, 1343 (2015).

[24] H. Baek, C.-H. Lee, K. Chung, and G.-C. Yi, Nano Lett. **13**, 2782 (2013).

[25] M. B. Sreedhara, K. Vasu, and C. N. R. Rao, Z. Anorg. Allgemeine Chem. **640**, 2737 (2014).

[26] Z. Y. Al Balushi, K. Wang, R. K. Ghosh, R. A. Vilá, S. M. Eichfeld, J. D. Caldwell, X. Qin, Y.-C. Lin, P. A. DeSario, G. Stone *et al.*, Nat. Mater. **15**, 1166 (2016).

[27] J. Li, Z. Shan, and E. Ma, MRS Bull. **39**, 108 (2014).

[28] T. Zhu and J. Li, Progr. Mater. Sci. **55**, 710 (2010).

[29] C. Lee, X. Wei, J. W. Kysar, and J. Hone, Science **321**, 385 (2008).

[30] S. Bertolazzi, J. Brivio, and A. Kis, ACS Nano **5**, 9703 (2011).

[31] K.-A. N. Duerloo, Y. Li, and E. J. Reed, Nat. Commun. **5**, 4214 (2014).

[32] Z. Zhu, Y. Cheng, and U. Schwingenschlögl, Phys. Rev. B **85**, 235401 (2012).

[33] W. Liu, X. Peng, C. Tang, L. Sun, K. Zhang, and J. Zhong, Phys. Rev. B **84**, 245105 (2011).

[34] H. Aramberri and M. C. Muñoz, Phys. Rev. B **95**, 205422 (2017).

[35] S. Liu, Y. Kim, L. Z. Tan, and A. M. Rappe, Nano Lett. **16**, 1663 (2016).

[36] J. Kalikka, X. Zhou, E. Dilcher, S. Wall, J. Li, and R. E. Simpson, Nat. Commun. **7**, 11983 (2016).

[37] S. J. Clark, M. D. Segall, C. J. Pickard, P. J. Hasnip, M. J. Probert, K. Refson, and M. Payne, Z. Kristall. **220**, 567 (2005).

[38] J. P. Perdew, K. Burke, and M. Ernzerhof, Phys. Rev. Lett. **77**, 3865 (1996).

[39] S. Grimme, J. Comput. Chem. **27**, 1787 (2006).

[40] S. P. Ong, W. D. Richards, A. Jain, G. Hautier, M. Kocher, S. Cholia, D. Gunter, V. L. Chevrier, K. A. Persson, and G. Ceder, Comp. Mat. Sci. **68**, 314 (2013).

[41] P. Blaha, K. Schwarz, G. Madsen, D. Kvasnicka, and J. Luitz, WIEN2K, *An Augmented Plane Wave + Local Orbitals Program for Calculating Crystal Properties*; Technische Universität Wien, Wien (2001).

[42] A. D. Becke and E. R. Johnson, J. Chem. Phys. **124**, 221101 (2006).

[43] F. Tran and P. Blaha, Phys. Rev. Lett. **102**, 226401 (2009).

[44] See Supplemental Material at http://link.aps.org/supplemental/10.1103/PhysRevMaterials.1.024003 for Figures 1S and 2S.

[45] J. A. Camargo-Martínez and R. Baquero, Phys. Rev. B **86**, 195106 (2012).

[46] S. W. Hwang and S.-H. Choi, Bull. Korean Chem. Soc. **37**, 1004 (2016).

[47] Y. Gohda and S. Tsuneyuki, Appl. Phys. Lett. **100**, 053111 (2012).

[48] D. Ruzmetov, K. Zhang, G. Stan, B. Kalanyan, G. R. Bhimanapati, S. M. Eichfeld, R. A. Burke, P. B. Shah, T. P. O'Regan, F. J. Crowne *et al.*, ACS Nano **10**, 3580 (2016).

[49] A. Yamada, K. Ho, T. Maruyama, and K. Akimoto, Appl. Phys. A: Mater. Sci. Proc. **69**, 89 (1999).

[50] P. Gupta, A. Rahman, S. Subramanian, S. Gupta, A. Thamizhavel, T. Orlova, S. Rouvimov, S. Vishwanath, V. Protasenko, M. R. Laskar *et al.*, Sci. Rep. **6**, 23708 (2016).